Mathematical Model of Steam Drying of Wood Chips and Other Hygroscopic Porous Media

Christian Fyhr and Anders Rasmuson
Dept. of Chemical Engineering Design, Chalmers University of Technology, S-412 96 Gothenburg, Sweden

A model is presented that is focused on the drying kinetics of single wood chips as a function of time and external conditions, such as temperature, pressure and velocity of the superheated steam. A multiphase and 2-D approach was used to model the coupled transport of water, vapor, air and heat in anisotropic hygroscopic porous media. The model was verified by drying experiments where measurements of the average moisture content, center temperature and pressure in a single wood chip could be performed simultaneously. A comparison between the calculations and the measurements showed that the drying behavior was well predicted. The drying can be divided into three stages: a heat-up period when condensation on the surface initially increases the moisture content; a period of constant drying rate when the external heat transfer controls the drying rate; and a period of decreasing drying rate when the drying is controlled by internal mass transfer. Many interesting features of the drying could be assigned to the strong anisotropicity of wood, which makes a 2-D model necessary.

Introduction

Interest in biofuels has increased recently. The main advantage of these fuels over the fossil ones is that there are no net CO_2 and SO_2 emissions. One common form of biofuel is wood chips, which are a by-product of the forest industry. Wood chips stored in piles before drying and combustion, contain about 75% water, on a dry basis, which makes drying necessary in order to achieve effective combustion.

Traditionally the drying medium has been hot air; however, the use of superheated steam is increasing (Wimmerstedt, 1994). Although the benefits of using this drying medium are mainly economic (reuse of the latent heat of steam), the inert atmosphere also reduces the fire hazards and, since the exhaust steam may be condensed, purification is easier than in the case of air drying.

There are several different types of equipment that are suitable for superheated steam drying. Some examples are the fixed-bed dryer, pneumatic conveying dryer, and fluid-bed dryer. When a pneumatic conveying dryer is used, the drying medium is steam at pressures higher than atmospheric. The pieces of wood are small, so that they can be conveyed by the steam. If the material fed to the dryer is colder than the saturation temperature of steam, condensation will occur, which leads to an initial increase in moisture content. The conditions occurring in a pneumatic conveying dryer will be our main focus. For design purposes, it is of great importance to know how the drying rate of a single particle is affected by the velocity, temperature, and pressure of the superheated steam.

Wood may be considered as a three-phase mixture consisting of solid cell walls with liquid water, air, and water vapor filling the lumen spaces. The water exists as free liquid above, and is bound to the cell wall below the fiber saturation point. During the drying process, flow of liquid, gas, and heat occurs due to gradients in pressure, water content, and temperature. Because of the strong anisotropicity of wood, the magnitudes of these flows are very dependent on the direction. This suggests that a multiphase and multidimensional model is required to solve the problem.

A literature search yielded several models for the drying of wood (Spolek, 1981; Plumb et al., 1985; Stanish and Schajer, 1986; Perré and Degiovanni, 1990). Most of them are focused on one-dimensional air drying of wood planks at atmospheric pressure; only a few are based on fundamental physics. The work presented here is concentrated on the development and experimental verification of a two-dimensional (longitudinal and transversal directions) model and simulation tool that takes into account the most important phenomena present during superheated steam drying of wood chips. The output

Correspondence concerning this article should be addressed to A. Rasmuson

of the model is the drying rate as a function of time and external steam conditions as well as internal distributions of moisture, temperature, and pressure. The model is easily generalized to account for air drying. It is envisaged that the model may be used for other hygroscopic materials with appropriate specification of material data.

Transport Processes

Drying is a process of simultaneous mass and energy transport occurring both inside and outside the piece of particulate material. In the case of wood, three moisture phases have to be accounted for: free (liquid) water, bound water, and water vapor. Evaporation rates are determined locally by the interaction of heat flows, temperature changes, and moisture flows.

Water in Wood. Moisture in wood can exist in three different forms: as free liquid in the cell cavities, X_f, as bound water in the cell walls, X_b, or as vapor in the gas phase. Due to the low density of the gas phase, the contribution of vapor to the total moisture content is often disregarded. The boundary between bound and free water is called the fiber saturation point, X_{FSP}, which is dependent on the temperature approximately as (Siau, 1984):

$$X_{FSP} = 0.325 - 0.001T. \tag{1}$$

Equilibrium Moisture Content. Due to the hygroscopicity of wood, an equilibrium between the bound water and the surrounding gas is established. The dependency of this equilibrium of temperature and activity of the steam has been investigated by Björk and Rasmuson (1995). The sorption forces that hold the water to the cell wall decreases the enthalpy of the bound water. The heat of sorption is equal to zero at X_{FSP} and increases as the moisture content approaches the equilibrium moisture content. The enthalpy of bound water is then equal to the enthalpy of free water less the enthalpy of sorption, as in the following equation (Stanish and Schajer, 1986):

$$h_b = h_{free}(T) - 0.4\Delta H_{vap}[(X_{FSP} - X_b)/X_{FSP}]^2. \tag{2}$$

External Heat Transfer. Heat is transferred from the surrounding steam to the surface of the wood chip by convection. Since the fluid stream impinges on the edge, small vortices may form just behind the leading edge, due to the finite thickness of the chip. Sorensen (1969) investigated the mass-transfer coefficients of truncated slabs and obtained the following correlation (expressed in heat transfer terms).

$$St = \frac{h}{\rho v C_p} = 0.152 Re_b^{0.179}[Re_x - 49.8 Re_b^{0.61}]^{-0.5} \tag{3}$$

$$250 < Re_b < 16{,}000 \qquad 2 < Re_x < 10^5.$$

The blunt edged plate expression predicts higher local heat-transfer coefficients close to the edge than the ordinary expression for flat plates. This is explained by turbulence production as the flow passes by the edge of the truncated slab.

Radiation is modeled according to the Stefan–Boltzman law, where the emissivity for spruce is assumed to be the same as for oak, for which the value 0.9 was found (Perry, 1973).

Internal Heat Transport. The most important mechanism for heat transport within a material during drying is conduction, which is modeled according to the Fourier law

$$\boldsymbol{q} = -k_{eff}\nabla T. \tag{4}$$

The effective heat-transfer coefficient, k_{eff}, is a combination of the heat-transfer coefficients of the three different phases; it is obtained experimentally (Siau, 1984) and is strongly dependent on the moisture content. Heat is also transported by convection, as mass transport occurs simultaneously. This is modeled by weighting the mass fluxes with the appropriate enthalpies (see Eq. 11). The ratio of longitudinal to transverse thermal conductivity for wood has been found experimentally to be approximately 2.5 (Siau, 1984).

External Mass Transfer. For drying in superheated steam, there is no resistance to mass transfer present at the surface. The convective transport of vapor across the surface equalizes the pressure between the surface and surroundings. The model can easily be extended to take external resistance for mass transfer into account (i.e., air drying). This can be accomplished by inserting a convective mass-transfer expression similar to the external heat transfer at the surface.

Internal Mass Transfer. The two-phase flow of fluids through porous media is described by an extended Darcy's law (Dullien, 1979)

$$\boldsymbol{n}_\alpha = -\rho_\alpha K \frac{k_\alpha}{\mu_\alpha}(\nabla P_\alpha - \rho_\alpha \boldsymbol{g}), \tag{5}$$

where $\boldsymbol{n}$ is the flux, K is the saturated permeability, k_α the relative permeability, and μ the viscosity of phase α. The gravitational term, $\boldsymbol{g}$, may be disregarded in vapor flow due to the small value of the density. The relative permeability is dependent on the saturation and on the porous material. In wood, flow of liquid occurs only above the fiber saturation point, where free liquid is present. The gaseous phase is mobile at all moisture contents except near full liquid saturation. For an anisotropic medium such as wood, the relative permeability becomes a tensor of the second order. Typically, the ratio K_L/K_T is of the order 10^3 for softwood (Siau, 1984). The pressures in each phase are coupled through the relation:

$$P_g - P_l = P_c, \tag{6}$$

where P_c is the capillary pressure that arises from surface tension effects at the liquid–gas interphase.

In addition to flow, diffusive transport of both the gaseous and liquid phases may take place. Gaseous diffusion is negligible in the case of steam drying but may be of importance in air drying. Bound water is mobile due to surface diffusion effects (Skaar and Babiak, 1982), and the transport of bound water is modeled according to Ficks law:

$$\boldsymbol{n} = -D_{BW}\nabla X \tag{7}$$

where n is the mass flux due to diffusion, ∇X is the gradient in moisture content, and D_{BW} is the effective diffusion coefficient. In steam drying, the main resistance to the diffusion of bound water is in the cell wall. The diffusion coefficient of bound water in the cell wall is strongly dependent on both temperature and moisture content.

Detailed expressions for the transport parameters in the preceding equations are given in the Appendix.

Mathematical Model

Assumptions and simplifications

The assumptions used in the steam-drying model for wood chips are:

- Transport is restricted to two directions (longitudinal and transversal directions)
- Wood is treated as homogeneous
- Local thermodynamic equilibrium is present between the three phases
- Bulk convection of the liquid and gas phases follows Darcy's extended law
- Bound water may migrate due to surface diffusion
- Shrinkage of the solid skeleton at low moisture contents is not taken into account
- The model does not allow for Knudsen diffusion, or hysteresis in either capillary pressure or relative permeability.

Governing equations

The mass balance for each component κ (water and air in general) becomes

$$\frac{\partial M^{\kappa}}{\partial t} = \nabla \cdot \left(\sum_{\alpha = l,g} \boldsymbol{n}_{\alpha}^{\kappa} \right). \tag{8}$$

The mass fluxes $\boldsymbol{n}_{\alpha}^{\kappa}$ are defined in Eqs. 5 and 7. The mass accumulation terms are the sums over phases

$$M^{\kappa} = \epsilon \sum_{\alpha = l,g} S_{\alpha} \rho_{\alpha} x_{\alpha}^{\kappa} \tag{9}$$

The saturation, S, of phase α is the fraction of the total void space (ϵ) filled with α, and the relation between the liquid saturation and moisture content is defined as

$$X = \frac{S_l \epsilon \rho_l}{(1-\epsilon)\rho_{\text{wood}}}. \tag{10}$$

The water below the FSP is treated as bound water. Heat is transported by convection and conduction and the heat balance is written as

$$\frac{\partial H}{\partial t} = \nabla \cdot \left(\sum_{\alpha = l,g;\, \kappa = w,a} h_{\alpha}^{\kappa} n_{\alpha}^{\kappa} - k_{\text{eff}} \nabla T \right), \tag{11}$$

where the heat-accumulation term contains both solid and fluid contributions

$$H = (1-\epsilon)\rho_{\text{wood}} Cp_{\text{wood}} T + \epsilon \sum_{\alpha = l,g} S_{\alpha} \rho_{\alpha} u_{\alpha} \tag{12}$$

Equations 8 and 11 are strongly coupled due to the interdependence of heat and mass flow, and they are highly nonlinear, due to the strong dependence of material properties on temperature and moisture content.

Initial and boundary conditions

The initial conditions were set to be as similar to the experimental ones as possible. Accordingly, the initial moisture content was set to 1.1 kg water per kg oven-dry wood for dense wood (density = 500 kg/m^3) and 1.6 for light wood (density = 400 kg/m^3), while the pressure was 1 bar. It must be noted that wood chips usually have a lower moisture content (about 0.75); however, since it is much easier to adjust the initial value in the simulations than to dry the fresh wood used in the experiments, the initial moisture content for fresh wood was used. The wood chips are initially at room temperature but, due to the experimental startup procedure, the chips are exposed to some heating before the drying starts. The initial temperature was therefore set to 60°C throughout the chip. The void space is initially filled with air in order to specify the initial conditions (pressure and temperature). After a short drying time, the air is replaced by steam. The pressure at the boundaries is set to the pressure of the surrounding steam. The temperature boundary is of the Neuman type and the heat flux at the surface is the sum of the convective (Eq. 1) and radiative contributions.

Solution of the equations

A model including general features for transport in porous media was developed by Pruess (1987) at Lawrence Berkeley Laboratories using the method of control volumes. This computer code, called TOUGH (Transport Of Unsaturated Groundwater and Heat), was originally written for geothermal applications. Since the governing equations are similar to those used in drying, this code forms the basis for the present work. The TOUGH code was extended to account for vapor pressure reduction and bound water diffusion. The properties of water below the FSP were set to those for bound water, and an enthalpy of sorption of water to the solid phase was introduced. Some minor modifications were also made to incorporate the transport properties of wood. An irreducible saturation of the gas phase was introduced in order to avoid total saturation of the liquid phase that causes major numerical problems. The irreducible saturation was accomplished by setting the relative permeability to zero when the liquid phase approached full saturation. The limit for liquid saturation was set to 0.999, which is high enough to have a negligible effect on the calculations. If the initial temperature of the wood is lower than the saturation temperature of steam at the existing pressure, condensation will occur. An extra element was introduced between the wood element and boundary element in order to model this phenomenon. This "surface element" is initially filled with steam at the same state as the surrounding steam and has very large heat conductivity in order to equilibrate the temperature between the "surface element" and the wood elements. The condensation of steam in the surface element then continues until the temperature of the

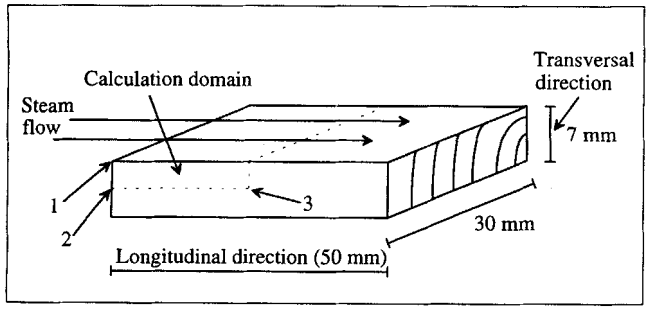

Figure 1. Dimensions of the wood chip.

adjacent wood element has reached the saturation value. A thin film of water is formed at the surface, this film disappears from the surface element by evaporation or is sucked into the wood by capillary action. This physical effect is to the authors' knowledge, neglected in previous models.

Numerical Study

Calculation domain and grid

The dimensions of the wood chip used in the present study are depicted in Figure 1. The size is somewhat larger than what would probably be used in practical drying, but was chosen in order to simplify the experiments.

Flow is modeled as passing through the surfaces perpendicular to the longitudinal and transversal directions. The transversal direction is included since the exchange surface perpendicular to this direction is the largest one. The permeability in the longitudinal direction is about 1,000 times higher than the transversal one, and is therefore accounted for. The third direction has the same permeability as the transversal direction, but has a much smaller exchange surface and in order to reduce the calculation time, flow in this direction was neglected. The area of the surfaces in the neglected direction is about 17% of the total surface. Due to symmetry, only one quarter of the wood chip is modeled. There are three different points marked in the figure. Point 1 is the corner of the chip, point 2 is located on the surface perpendicular to the longitudinal direction and point 3 is located in the center of the chip. These points will be referred to later in the discussion of different drying features. The transversal and longitudinal directions are discretized into 20 elements each, which gives a grid with totally 400 control volumes. In order to test the grid dependence, a test for drying case E (see Table 1), with the number of elements in the transversal direction increased to 30, was performed. The comparison showed that the total drying rate and overpressure at the center were affected only in the third decimal.

Drying cases

The simulated drying cases are found in Table 1. The permeabilities for all cases were set to be approximately valid for spruce wood, Picea Abies ($K_L = 5 \cdot 10^{-13}$, $K_T = 5 \cdot 10^{-17}$). Since the pressure in a pneumatic conveying dryer varies in the direction of the flow, the pressure in the simulations is varied between 1 and 3 bar, where 3 bar represents the pressure of the inlet steam. The temperature in the dryer is assumed to be between 150 and 180°C.

Table 1. Drying Cases

Case	Pres. bar	Temp. (°C)	Slip Vel. m/s	Heat Flux (W/m^2)
A	1	150	1	1,550
B	1	150	2	2,170
C	1	170	1	2,230
D	2	170	2	3,270
E	2	170	1	2,280
F	3	170	1	2,120
G	3	180	1	2,720

Experimental Study

Experimental setup

An experimental device for the simultaneous measurement of weight, center pressure, and temperature during the drying of single wood chips was developed (see Figure 2). The apparatus was built for pressures up to 10 bar, although no experiments above 3 bar were performed. The steam is produced in an electrically heated boiler (maximum 10 bar, 25 kg/h), and the superheating is performed in a superheater with a heating coil connected to a control circuit. An additional heating circuit is placed inside the measuring compartment in order to compensate for heat losses. By means of these control circuits, the temperature could be kept at any point between 100 and 200°C with an accuracy of ± 1°C. The pressure was controlled by a back-pressure valve located

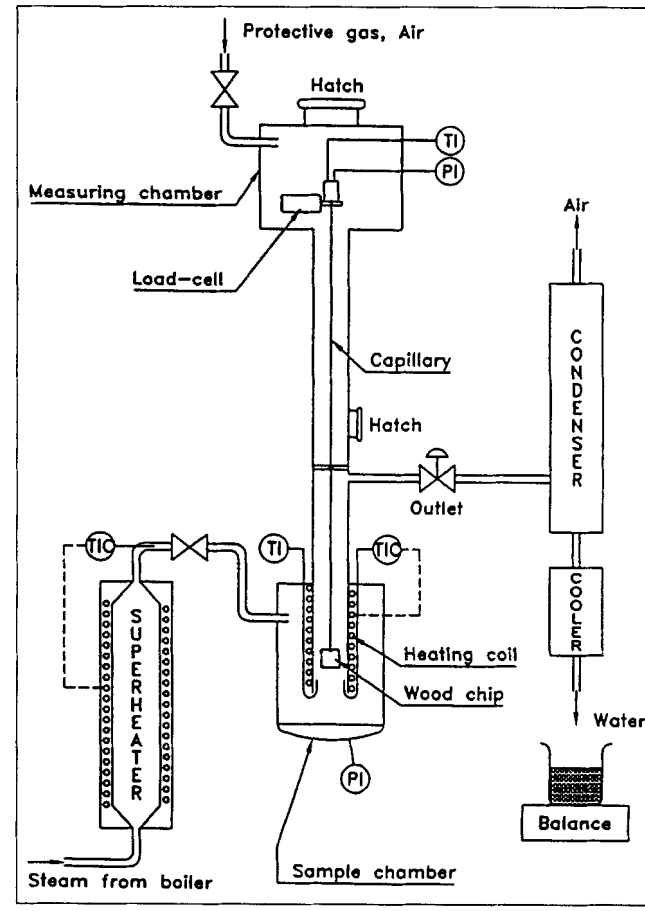

Figure 2. Experimental setup.

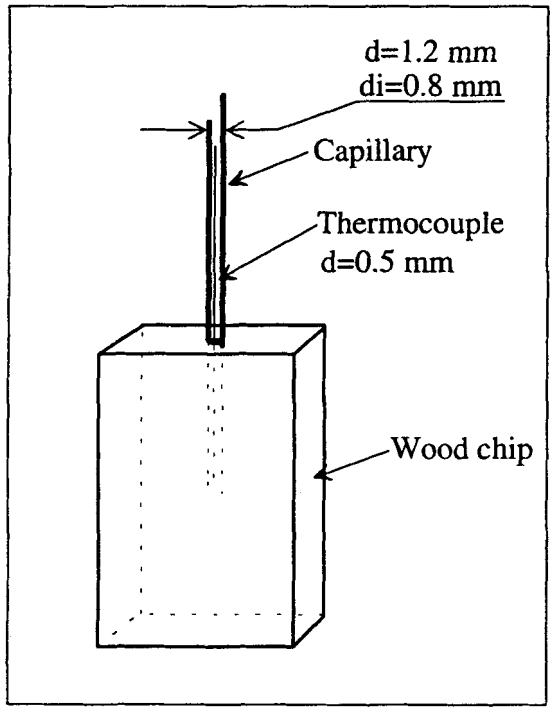

Figure 3. Intrinsic pressure and temperature.

downstream of the sample compartment. Due to variations of the pressure in the boiler, the pressure in the sample compartment was oscillating about 1.5% around the set value. However, the average pressure could be controlled at less than 0.01 bar from the set value. The pressure was measured by a pressure transducer located just below the wood chip. In order to control the mass flow of steam (and thereby the steam velocity that passes by the wood chip), the pressure in the boiler was set to a value slightly higher than that at the outlet valve. The mass flow was then obtained by condensing the outlet steam and collecting the cooled water on a balance. Although the mass flow was oscillating for the same reason as the pressure, the average value could be adjusted to be very close to the one set ($\pm 2\%$). Since the load cell in the measuring chamber is sensitive to moisture and high temperatures, protective gas (compressed air) is blown through this compartment and exits at the same outlet as the steam.

The wood chip is mounted on a capillary tube as depicted in Figure 3. The end of the capillary is located in the center of the wood chip. A thermocouple is inserted through the capillary in order to measure the temperature in the center of a chip. The pressure in the center is transferred through oil in the space between the thermocouple and the capillary wall. The other end of the capillary is mounted on a load cell, which registers the weight loss during drying. The pressure is transferred through a Teflon tube filled with oil, to a pressure transducer inside the measuring chamber.

Typically, 10 experiments were performed for each drying case. The curves for moisture content and temperature were very reproducible. The overpressure curves showed more variety. This is due to the inhomogeneous nature of wood; it is impossible to perform experiments on identical wood chips since it is a biological material. The overpressure is strongly affected by variations in the permeabilities as discussed in the sensitivity analysis.

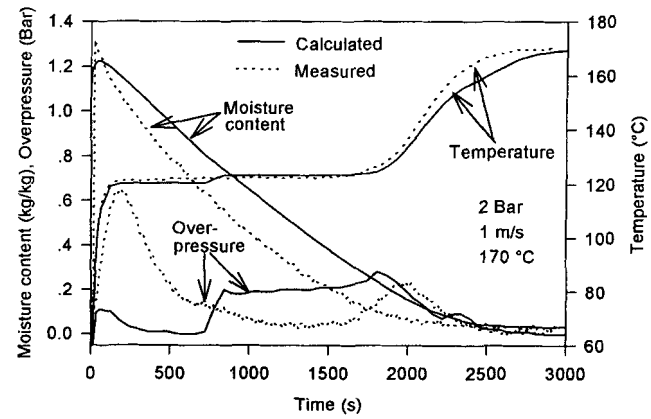

Figure 4. Comparison between experimental and simulated drying behavior for drying case E.

Results and Discussion

Numerical and experimental comparison

Comparison for Reference Case E. A direct comparison between the calculated and measured drying behavior for spruce is shown in Figure 4. It must be emphasized that all of the transport parameters used in the simulations were taken from the literature and that no information was taken from the measurements to obtain a better fit to the experiments.

From the figure it can be seen that the simulations and experiments have similar features. It cannot be expected that the drying curves will match exactly, since the initial moisture contents are not exactly the same and also the maximum drying rates are different due to the different sizes of the exchange surfaces. The latter discrepancy could be avoided by introducing a third dimension to the simulations. The number of control volumes would be very large, however, and this would lead to very long computing times. An attractive alternative method would be to multiply the heat-transfer coefficient by a factor of 1.17 in order to compensate for the difference in total surface area. This would provide correct drying rates in the constant rate period, but would cause deviations in the falling rate period. When comparing drying rates, it should also be noted that the unit moisture content is somewhat misleading since it is based on the loss of water per mass of dry weight. The dry weight is, however, different from one chip to another. Some investigators have put glue on the surfaces perpendicular to the third dimension. Although this prevents mass transfer through the surface, heat transfer will still occur. Anyway, examination of real wood chips shows that the surface perpendicular to the third direction is often very small due to the cutting process.

The overpressure curves exhibit somewhat more variety. The initial overpressure in the experiments is due to initial heatup of the air in the capillary and has no connection to the drying process. The plateau in the simulated pressure curve is due to a too large degree of anisotropicity in the permeabilities. The magnitude of the maximum overpressure is closely predicted for case E. This is a good indication that the permeabilities used in the simulations correspond to the real ones. It must be emphasized that only a small deviation in the permeability, especially in the longitudinal direction,

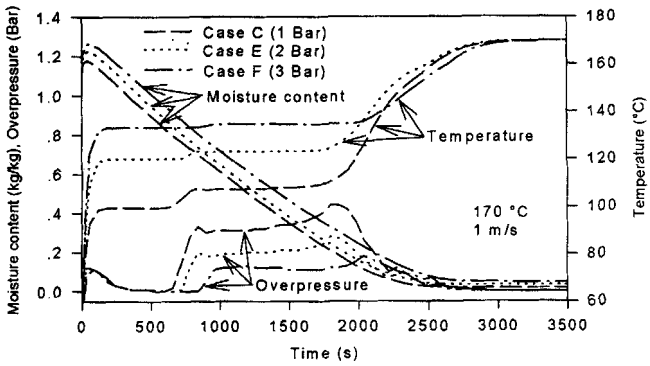

Figure 5. Effect of pressure on simulated drying results.

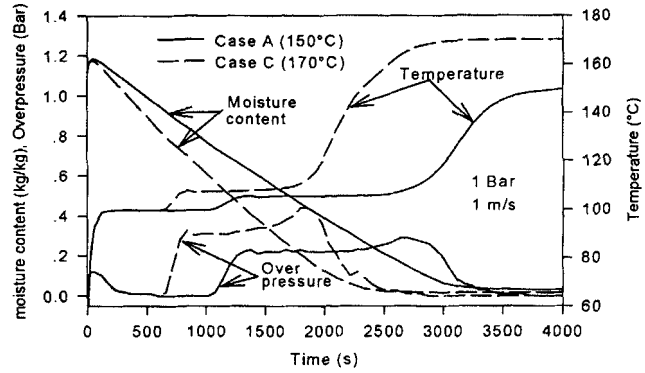

Figure 7. Calculated temperature dependence.

affects the overpressure significantly. This was also noted in the experiments, as some of the samples showed considerably less overpressure than the one in Figure 4.

The temperature curves are in good agreement. The close agreement during the heatup period indicates that the heat conductivity in the simulations is close to the values for the real wood, both in magnitude and in temperature dependence. The small discrepancy between the curves in the final heatup period may be explained by differences in heat transfer to the surface, by different distributions of the moisture or in the moisture dependence of the heat-transfer coefficient, or by a combination of these. An additional run for case E with somewhat adjusted parameters was performed. The transversal permeability was increased by a factor of 10 in order to obtain a smaller magnitude of maximum overpressure and to avoid the plateau. The smaller exchange area in the simulations was compensated for by simply increasing the heat flux to the surface by a factor of 1.17. With these small changes, the drying rates during the constant drying period are in good agreement.

The simulated drying behavior for three different pressures 1, 2, and 3 bar (drying cases C, E, and F) is depicted in Figure 5. The drying rates are approximately equal for all of the cases, and the discrepancies in total drying time are due to different amounts of condensation of steam during the heatup period. The drying during the constant-rate period proceeds at the boiling points (100, 120, and 133.5°C). The greater the difference between the boiling points and the temperature of the surrounding steam, the larger the overpressure, as shown in the figures. The measured results for the same drying cases are displayed in Figure 6. The tendencies are the same as in the calculations, with the exception that the overpressure for drying case C is less than predicted. This is probably due to variations in the wood chip quality.

To compare the temperature dependence, calculated and measured drying behavior for drying cases A and C are depicted in Figures 7 and 8, respectively. A comparison of these figures makes it is clear that the predictions are in fair agreement with the measurements. The drying for case A is significantly slower, which causes less overpressure and a less steep temperature curve during the final heatup period. The overpressures are, as before, less than predicted, for the reasons discussed earlier.

An increase in the steam velocity from 1 to 2 m/s reduces the drying time significantly. This is depicted in Figure 9, where the drying of soft spruce for drying cases D and E is compared. The measured results for the same drying cases are shown in Figure 10. In order not to interfere with the drying curves, the pressure curves have been increased by adding 0.5. By comparing the calculated and measured drying behavior, it can be seen that the general trends are the same, although the calculated displacements between the pressure and temperature curves are larger than those of the measured ones. The difference between the maximum overpressures is due to reasons already discussed; however, the displacement between the calculated temperature curves is more notable. This indicates that the internal transports were predicted erronously, especially for drying case D. This case rep-

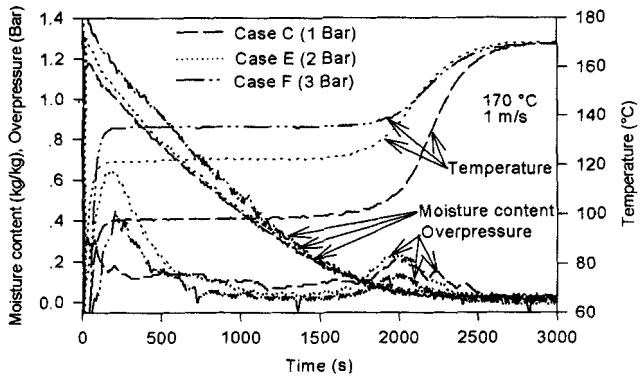

Figure 6. Effect of pressure on measured drying behavior.

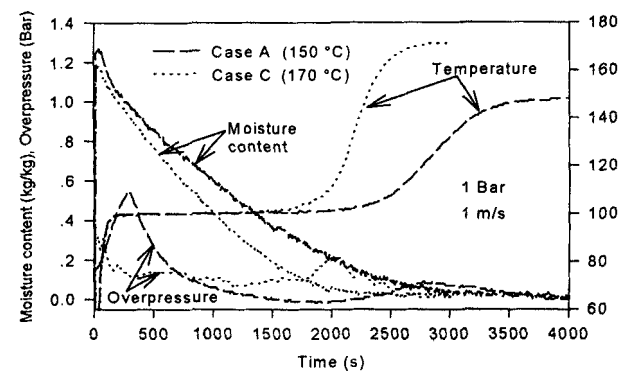

Figure 8. Measured temperature dependence.

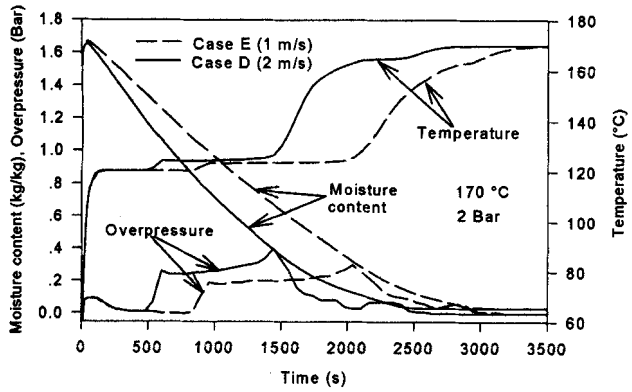

Figure 9. Calculated steam velocity dependence.

resents the hardest drying conditions with the highest heat transfer; consequently, the drying is internally controlled during the main part of the drying sequence. An error in the transversal permeability will then become more obvious. An additional run with the transversal permeability increased by a factor 10 also showed considerably less displacement between the simulated and measured curves.

Simulated drying behavior

Drying Rates. The drying rates for all of the drying cases in Table 1 are shown in Figure 11. A period of constant drying rate, which starts after about 200 seconds, is clearly visible for all of the drying cases. The length of this period varies considerably. This is mainly because of the different drying rates, but it is also due to different mobilities for the liquid phase: the liquid viscosity is strongly dependent on the temperature. When the surface enters the hygroscopic range, the drying rate decreases rapidly, as it is then controlled by the mass transfer inside the material. A small increase in drying rate is seen after the first sharp decline. This is due to the internal overpressure, which drives moisture toward the small surface and causes the drying rate to increase. This effect is stronger for the cases with harder drying conditions, but it does not have a significant effect on the total drying time. It can be seen in Figure 11 that a certain increase in the maximum heat transfer rate does not necessarily lead to an equivalent shortening of the total drying time. The ratio between the maximum drying rates for cases G and A is 1.7; however,

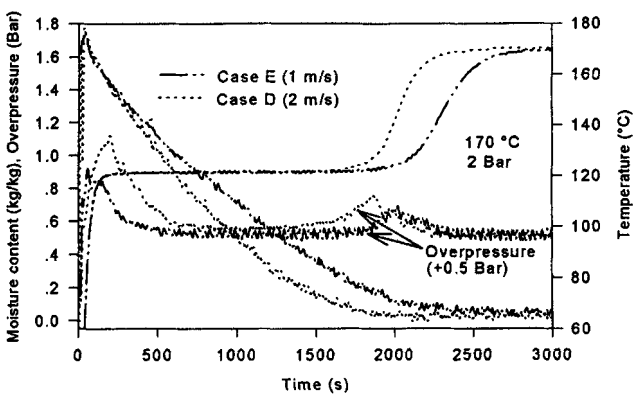

Figure 10. Measured steam velocity dependence.

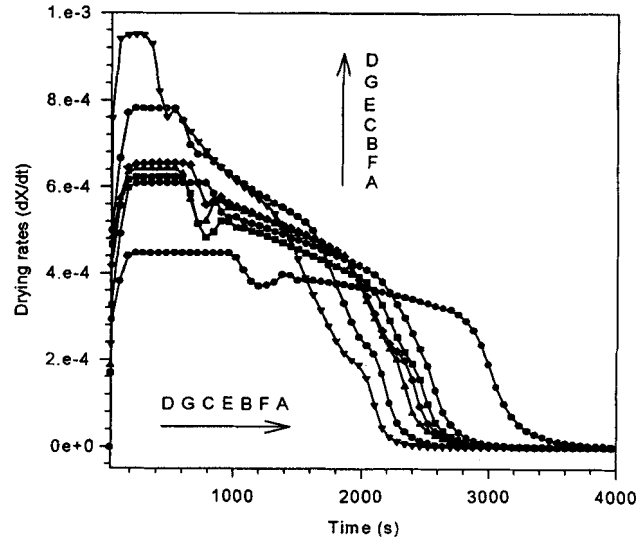

Figure 11. Drying rates for seven cases.

the ratio of the total drying time is only 1.4, which indicates that the total drying time is not determined by the heat-transfer rate alone. Another striking example is the drying for cases E and C, where case E has the largest heat-transfer rate but the total drying time is shorter for case C. Since the temperature difference between the boiling point and the surrounding steam is larger for case C, the internal overpressure becomes larger for this case, which enhances the drying rate in the second drying period.

General Drying Behavior. The general behavior for drying case E is depicted in Figure 12. The moisture content increases initially due to the condensation of steam on the surface, as well as inside the material. Since the initial pressure inside the particle is 1 bar, the surrounding steam is forced into the chip where it condenses and increases the moisture content. The pressure is equalized in about 20 s. The temperatures at these different points are also plotted in Figure 12. The locations of these points are illustrated in Figure 1. Point 1 is located on the edge of the chip, point 2 is located on the surface perpendicular to the longitudinal direction, and point 3 in the center of the material.

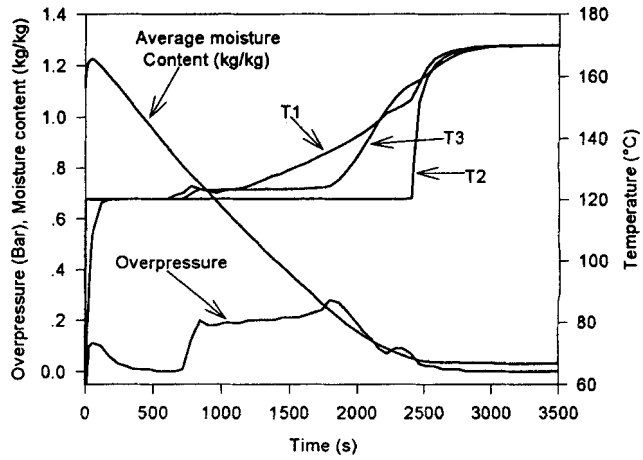

Figure 12. General drying behavior.

The temperatures increase rapidly up to the boiling point and remain there during the period of constant drying rate. When the liquid transport at the surface is no longer sufficient to consume the heat transferred by evaporation, the temperature rises above the boiling point. Since point 1 is located at the edge, the temperature rises first at this point. Note that the temperature at point 2, although it is located on a surface, is held at the boiling point for a longer time than at point 3, which is located in the center of the material. This indicates that the moisture content is higher at point 2. This phenomenon is discussed more thoroughly in the next section. The overpressure at the center of the material is also plotted in Figure 12. Since the overpressure is a function of the temperature, it starts to rise simultaneously with the rise in temperature at the center. The surface enters the hygroscopic range at about 700 s, causing the temperature and, accordingly, the pressure to rise throughout the material. The overpressure reaches its maximum value at about 1,860 s, and then declines as the moisture content falls below the FSP.

Another way of illustrating the drying behavior is by plotting the pressure vs. the temperature at the center of the material. This method, called Identity Drying Card (IDC), was developed by Perré (1994), and the plot obtained displays several features of both the drying medium and the drying material. One such plot for drying case E is depicted in Figure 13.

The points to the left of the saturation curve represent the initial heating period (0–200 s in Figure 12), where a small overpressure with a maximum at about 0.1 bar is built up. When the temperature and pressure at a given point are in equilibrium, the dots lie on the saturation curve. The pressure then increases rapidly as the temperature rises and reaches a maximum at which the moisture content is at the FSP. The magnitude of the overpressure is a measure of the permeability of the material. The material then enters the hygroscopic range where the overpressure declines toward zero.

The Detailed Evolution of Moisture Content, Pressure, and Temperature Distributions. Figures 14a to 14e illustrate the moisture content distributions at different times for drying

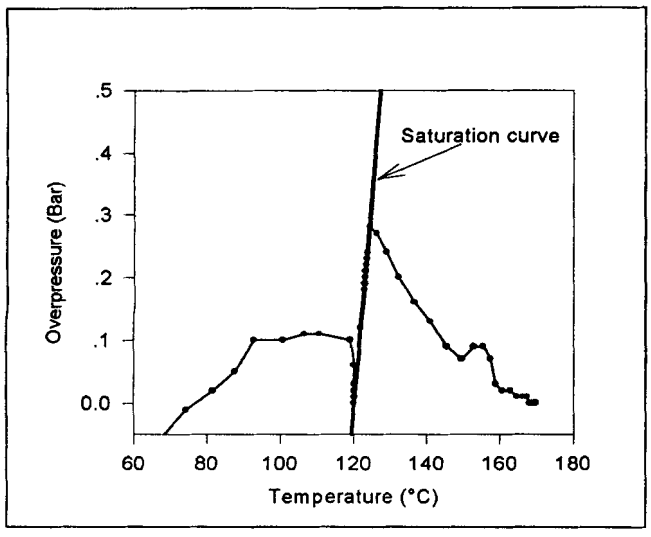

Figure 13. IDC plot for drying case E.

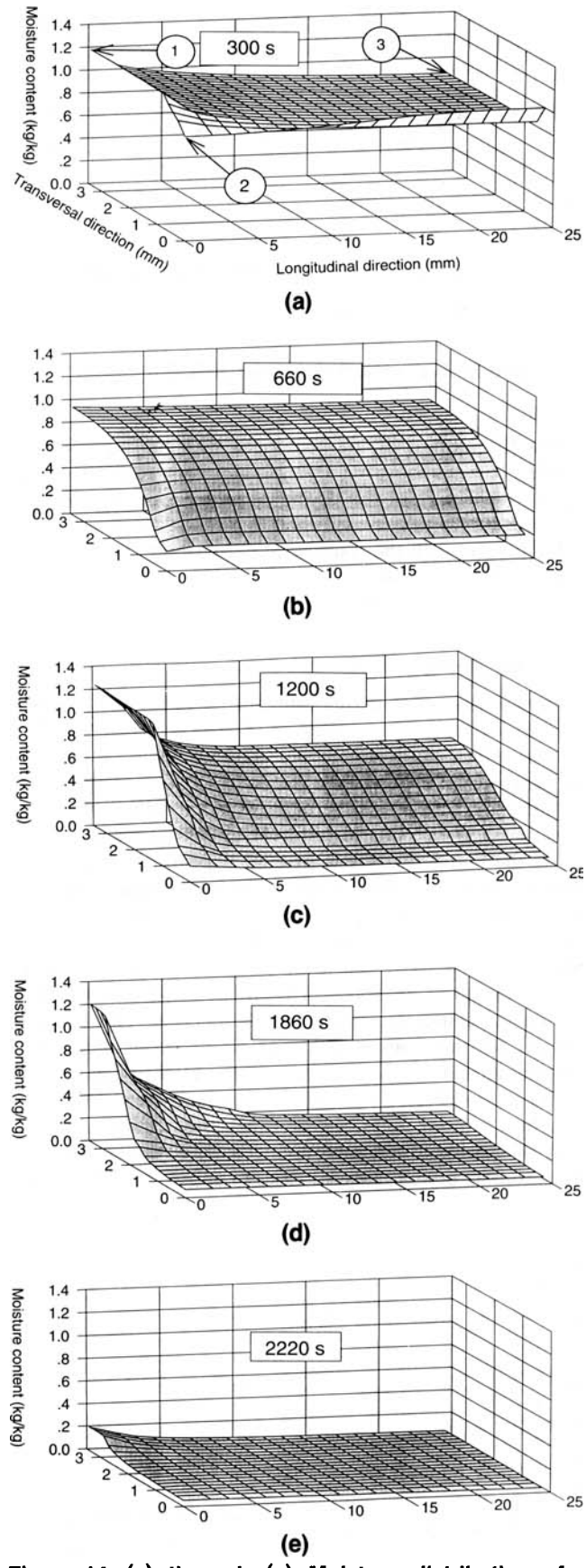

Figure 14. (a) through (e) Moisture distributions for drying case E.

case E. Three different points are denoted in Figure 14a. Point 1 is located on the edge of the chip, point 2 on the surface perpendicular to the longitudinal direction, and point 3 in the center of the chip as described earlier in Figure 1. In Figure 14a (300 s) it can be seen that the drying starts first at the edge. The combined effects of the initial overpressure, which drives the moisture to the surfaces, and the condensation on the surface during the heatup period lead to an accumulation of moisture at the surfaces. After 660 s (Figure 14b), the large surface perpendicular to the transversal direction starts to dry out and, at 1,200 s (Figure 14c), the moisture content at this surface has reached the equilibrium value. Here, a gradient in moisture content in the longitudinal direction can be seen. In fact, the moisture content at point 2, although this point is located at a surface, is greater than at the center of the material, point 3. This is the reason why the temperature at point 2 was held at the boiling point for a longer time than at point 3, as seen in Figure 12. At 1,860 s (Figure 14d), the gradient in moisture content in the longitudinal direction is even stronger, as the moisture content at the surface is still held at the saturation value and the moisture content at the center has reached the hygroscopic range. At 2,220 s (Figure 14e), there is only a small amount of moisture remaining in the vicinity of point 2.

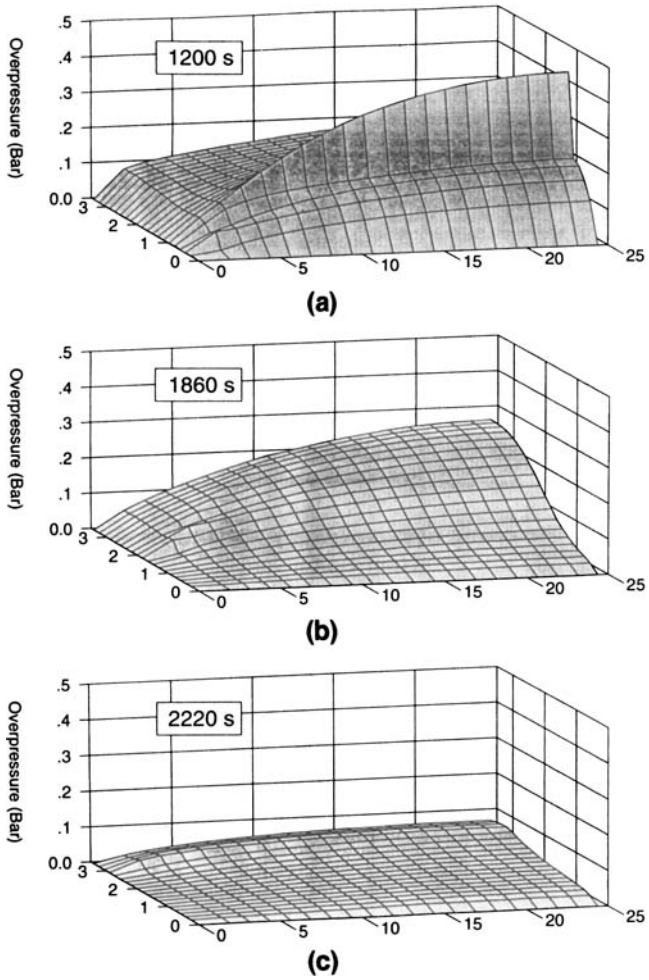

Figure 15. (a) through (c) Overpressure distributions for drying case E.

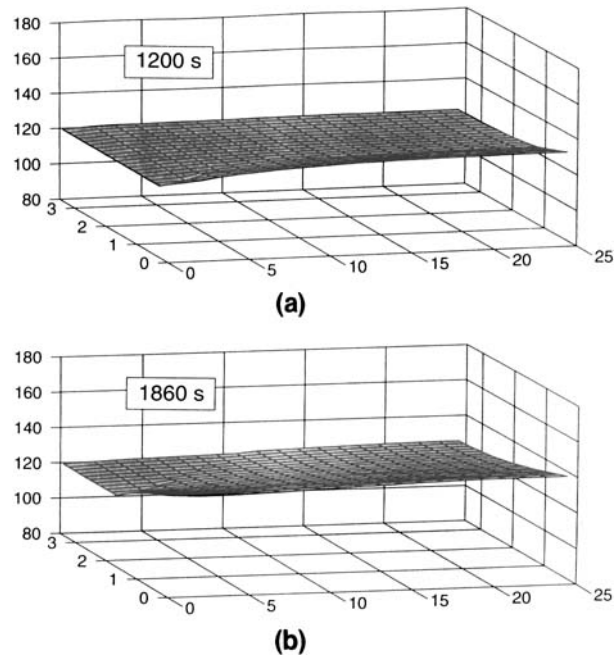

Figure 16. (a) and (b) Temperature distributions for drying case E.

The distributions of overpressure are depicted in Figures 15a–15c. The overpressure starts to rise at the surface first, as seen in Figure 15a. This is because the overpressure is a function of both temperature and moisture content. The temperature starts to rise first at the surface, as does the overpressure. The "hump" in overpressure then moves toward the center, as shown in Figure 15b and Figure 15c. At 1,860 s (Figure 15b), the overpressure has reached its maximum value at the center of the material where pressure gradients exist in both the longitudinal and transversal directions. In this circumstance, according to Darcy's law, flow of both liquid and gas occurs in the direction of highest permeability, which is the longitudinal one here. Consequently, the surface perpendicular to the longitudinal direction becomes enriched in moisture. This is the explanation for the lower temperature at this point. As the whole chip enters the hygroscopic range, the overpressure decreases, and at 2,220 s (Figure 15c), the pressure is approximately equal to that of the surroundings.

The temperature distributions for two different times are shown in Figure 16a–16b. Temperature gradients are only significant in the heating-up and falling-rate periods and are largest in the transversal direction. Similar figures could also be made for the other cases stated in Table 1. If the drying conditions are hardened, the different features of the profiles become more pronounced. For example, the moisture distributions for drying case C would exhibit stronger moisture gradients in both the transversal and longitudinal directions. The pressure distributions for the same drying case would show that the pressure evolution is very much the same but stronger in magnitude.

Mechanisms of heat and mass transport in each drying period

The relative importance of each flow mechanism in the transversal direction for drying case E is depicted in Figure

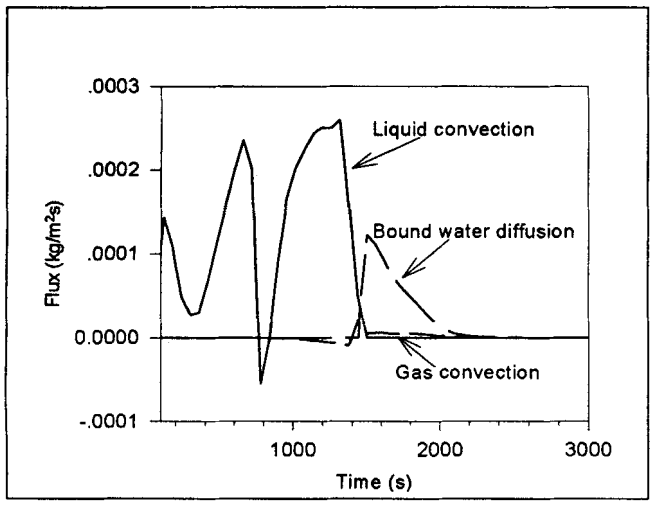

Figure 17. Flow mechanisms in the transversal direction.

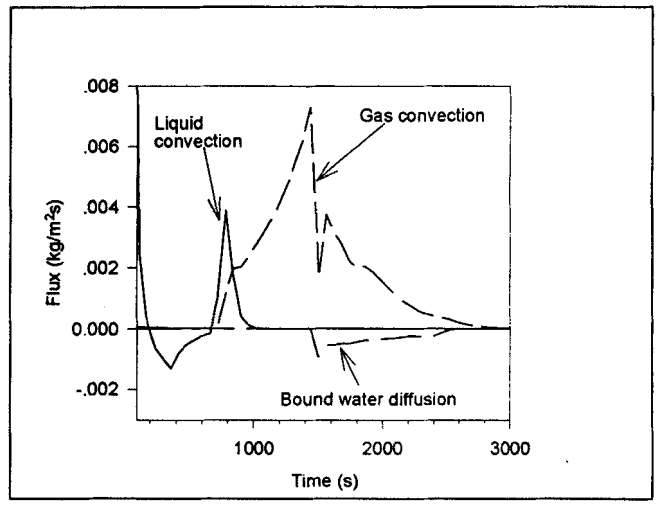

Figure 18. Flow mechanisms in the longitudinal direction.

17. These curves are valid for a point in the center of the calculation domain, and the flux is regarded as positive toward the surface. First, due to the small initial overpressure inside the material, liquid is pushed toward the surface during the first 100 s. Then, at about 200 s the flux reaches a minimum where the capillary pressure and total pressure almost equalize. During the period of constant drying rate, 250–600 s, the flux of liquid due to capillary action reaches a maximum. Between 750 and 1,000 s, the liquid convection exhibits a dip that is due to the fact that the hump in overpressure passes through this point. On the far side of this hump, the gradient in total pressure is counter to the gradient in capillary pressure and, at about 800 s, these gradients cancel each other causing zero water flux at this point. As the moisture content at this point approaches the fiber saturation point, the relative permeability of the liquid phase becomes zero and the liquid convection disappears.

The flow mechanisms for the point in the longitudinal direction are plotted in Figure 18. Here, it can be seen that the liquid convection is relatively less important in the longitudinal direction than in the transversal direction. The main mechanism for water transport is the convection of the gas phase. The magnitude of the gas convection depends on the overpressure as well as the permeability. The gas convection is higher in this direction due to the higher permeability. Since the gradients in moisture content are lower in this direction, diffusion of bound water becomes less important. The direction of the bound water diffusion is toward the center due to the gradients in moisture content. Points at other locations in the material display the same profiles as the figures just given, with the difference that they would be displaced in time.

Sensitivity to transport parameter values

In order to test the sensitivity of the model to deviations in the transport data, additional runs for drying case E were performed. The parameters that were varied are listed in Table 2. The level of uncertainty will probably be different for the various parameters, as indicated by the scaling factors in the second column of Table 2. In order to compare the effects of all of the different changes, the relative change in total drying time and maximum internal overpressure are tabulated.

The value of the bound water diffusion coefficient is clearly not critical for the drying. This is not surprising since diffusion of bound water is significant only in the transversal direction during the falling-rate period (Figure 17). The effect of a change in the coefficient for heat conduction is pronounced; since heat is then spread more efficiently and the mobility for mass is kept constant, the overpressure increases. The overpressure causes more vapor flow in the longitudinal direction, which enhances the drying rate during the second drying period. A change in the capillary pressure also has a major effect on the drying. The greater the capillary pressure, the greater is the ability to suck water to the surface during the constant-rate period, which extends the period. The total drying time is thus reduced when the capillary pressure is increased. The internal overpressure is also affected since the amount of moisture in the center of the material is different during the late part of drying, since the amount of water drawn to the surface by capillary action changes. The permeability of wood has a significant effect on drying. The drying time is reduced if the permeability is increased and this reduction is approximately the same for ei-

Table 2. Sensitivity in Drying Results Due to Uncertainties in Transport Parameters

Parameter	Scaling Factor	Rel. Change in Total Drying Time	Rel. Change in Internal Overpres.
D_{BW}	2	−0.5%	—
D_{BW}	0.5	+0.5%	—
k	1.5	−6.0%	+14%
k	0.67	+8.0%	−17%
P_c	2	−7.0%	−7%
P_c	0.5	+10.0%	+18%
K_T	10	−10.0%	−29%
K_T	0.1	+8.0%	+39%
K_L	10	−8.0%	−86%
K_L	0.1	+10.0%	+510%

ther longitudinal or transversal change. The change in internal overpressure, however, is much more sensitive to a change of the permeability in the longitudinal direction. It is notable that the overpressure increases by a factor of more than five, as the longitudinal permeability is divided by 10. This is explained by the fact that the essential part of the pressure release is in the longitudinal direction, so that a change in the transversal direction does not change the overpressure very much. However, the drying time is affected by a lower permeability in the transversal direction, since the length of the constant drying period becomes shorter as the ability to suck water to the surface decreases.

Conclusions

A comprehensive model for the drying of wood chips in superheated steam is presented in this work. The model is based on fundamental transport mechanisms and conservation laws; it gives the moisture content, pressure, and temperature at each point in a wood chip as a function of time and external conditions such as temperature, pressure, and velocity of the superheated steam.

An experimental device for the drying of single wood chips, which facilitates simultaneous measurements of average moisture content, center pressure, and temperature, as a function of time, was developed. The drying behavior for several different conditions was measured and the resulting curves for moisture content and center temperature showed good agreement with the simulations. The pressure curves were in fair agreement with the simulations.

The absolute permeabilities used in the simulations were somewhat too low. The clearest indication of this was that the internal overpressure was more or less overpredicted for all cases. Comparison of the drying curves and temperature curves indicated that the other transport parameters were in agreement with the real ones.

Drying can be divided into three stages: a heatup period, when condensation on the surface initially increases the moisture content; a period of constant drying rate, when the external heat transfer controls the drying rate; and a period of decreasing drying rate, when the drying is controlled by internal mass transfer.

The external heat transfer was found to have a significant influence on the total drying time. It was found that, while keeping the other parameters constant, an increase in steam velocity or temperature increases the drying rate significantly, whereas the steam pressure hardly affects the drying rate at all.

The mass transport during the first part of the drying is controlled by capillary suction of moisture to the surface in the transversal direction, where evaporation takes place. As the surface dries out, the temperature at the surface increases and an internal overpressure is built up. This overpressure drives moisture and gas in the longitudinal direction, and the net efflux of water then becomes controlled by flow through the small surface. Bound water diffusion was important only in the transversal direction, whereas gas convection in this direction was negligible. The pressure-induced flow in the longitudinal direction causes an accumulation of moisture at the smaller surface, which somewhat unexpectedly leads to lower temperatures at this surface than in the center of the wood chip. The features mentioned earlier can be assigned to the strong anisotropicity of wood, which makes a two-dimensional model necessary.

By considering the relevant uncertainties of the input parameters, a simple sensitivity analysis showed that a change in the heat conductivity, capillary pressure, or the permeability each has about the same influence on the total drying time. The value for the bound water diffusion coefficient, however, was not important for the overall drying time.

Notation

Cp = heat capacity, J/kg·K
h = heat-transfer coefficient, W/m^{2}K
h_b = enthalpy of bound water, J/kg
h_{free} = enthalpy of free water, J/kg
q = heat flux, W/m^2
Re = Reynolds number
St = Stanton number for heat transfer
T = temperature, K
u = internal energy, J/kg
v = velocity, m/s
ρ = density
ΔH = heat of vaporization
σ = surface tension, N/m

Indices and operator

b = thickness of wood chip
L = longitudinal direction
T = transversal direction
x = distance from leading edge
$\nabla\cdot$ = divergence

Literature Cited

Björk, H., and A. Rasmuson, "Moisture Equilibrium of Wood and Bark Chips in Superheated Steam," *Fuel*, **74**, 1887 (1995).

Dullien, F. A. L., *Porous Media, Fluid Transport and Pore Structure*, Academic Press, New York (1979).

Perré, P., and A. Degiovanni, "Simulation par Volumes finis des Transferts Couplés en Milieux Poreux Anisotropes: Séchage du Bois à Basse et à haute Température," *Int. J. Heat Mass Transfer*, **33**(11), 2463 (1990).

Perré, P., M. Moser, and M. Martin, "Advances in Transport Phenomena during Convective Drying with Superheated Steam and Moist Air," *Int. J. Heat Mass Transfer*, **36**(11), 2725 (1993).

Perré, P., "The Concept of Identity Drying Card," *Proc. Int. Drying Symp.*, Gold Coast, Australia (1994).

Perry, R. H., *Chemical Engineers Handbook*, McGraw-Hill, New York (1973).

Plumb, O. A., G. A. Spolek, and B. A. Olmstead, "Heat and Mass Transfer in Wood During Drying," *Int. J. Heat Mass Transfer*, **28**(9), 1669 (1985).

Pruess, K., *TOUGH User's Guide*, Univ. of California, Berkeley (1987).

Siau, J. F., *Transport Processes in Wood*, Springer-Verlag, Berlin (1984).

Skaar, C., and M. Babiak, "A Model for Bound Water in Wood," *Wood Sci. Technol.*, **16**, 123 (1982).

Sorensen, A., "Mass Transfer Coefficients on Truncated Slabs," *Chem. Eng. Sci.*, **24**, 1445 (1969).

Spolek, G. A., "A Model of Simultaneous Convective, Diffusive and Capillary Heat and Mass Transport in Drying Wood," PhD Thesis, Washington State Univ. (1981).

Stanish, M. A., and G. S. Schajer, "A Mathematical Model of Drying for Hygroscopic Porous Media," *AIChE J.*, **32**(8), 1301 (1986).

Wimmerstedt, R., "Steam Drying-History and Future," *Drying'94, Proc. Int. Drying Symp.*, Gold Coast, Australia (1994).

Appendix

All experimental samples were sawn out of fresh sapwood from spruce (Picea Abies).

Porosity:
soft spruce, $\epsilon = 0.73$
dense spruce, $\epsilon = 0.67$
Solid wood density: $\rho = 1{,}500$ kg/m^3
Heat capacity for solid wood: Cp = 1,400 J/kg·K
Heat conductivity (Perré et al., 1993):

transversal direction

$$k_T = (0.129 - 0.049X)(0.986 + 2.7X) \cdot (1 + (2.05 + 4X)(T - 273) \times 10^{-3}) \qquad X < 0.4$$

$$k_T = (0.0065/X + 0.0932)(0.986 + 2.7X) \cdot (3.55 + 3.65T) \times 10^{-3} \qquad X > 0.4$$

longitudinal direction $k_L = 2.5k_T$

Vapor pressure below X_{FSP} (vapor pressure lowering) (Björk and Rasmuson, 1995):

$$P_v = \Psi P_{v,\text{sat}}$$

$$\Psi = D + \sqrt{D^2 + A/B}$$

$$A = -9.94 + 2.45/X_{FSP}, \quad B = 58.17 - 7.69/X_{FSP}$$

$$C = 68.08 - 9.15/X_{FSP}, \quad D = -0.5(1/CX - C/B)$$

Permeabilities:
transversal direction, $K_T = 5 \cdot 10^{-17}$ m^2

Relative Permeabilities (Perré and Degiovanni, 1990)

	k_l	k_g
$X_l = 0$	0	1
$0 < X_l < 0.8$	$0.95\left(\frac{X_l}{0.8}\right)^2$	$0.95\left(1 - \frac{X_l}{0.8}\right)^2 + 0.05$
$0.8 < X_l < X_{\text{sat}}$	$0.05\frac{X_l - 0.8}{X_{\text{sat}} - 0.8} + 0.95$	$0.05\frac{X_{\text{sat}} - X_l}{X_{\text{sat}} - 0.8}$

where $X_l = X - X_{FSP}$ $X_{l,\min} = 0$.
longitudinal direction, $K_L = 5 \times 10^{-13}$ m^2

relative permeabilities (Perré et al., 1993)

$$k_l = X^{*3} \qquad \text{with} \qquad X^* = X_l/X_{\text{sat}}$$

$$k_g = 1 + (2X^* - 3)X^{*2}$$

Capillary pressure (Perré et al., 1993):

$$P_c = 1.364 \times 10^5 \sigma (X_l + 1.2 \cdot 10^{-4})^{-0.63}$$

Diffusion coefficient for bound water (Siau, 1984):

$$D_{BW} = 5 \cdot 10^{-4} \frac{D_w}{(1 - \beta)(1 - \sqrt{\beta})}$$

where D_w is the diffusion coefficient in the solid wood.

transversal direction:

$$D_{w,T} = 7 \times \exp((-9{,}200 + 7{,}000X)/RT)$$

longitudinal direction:

$$D_{w,L} = 250\beta D_{w,T}$$

$$\beta = 1 - 0.5(\epsilon + X) \qquad \beta_{\min} = 0 \qquad R = 1.987 \text{ kcal/kmol·K}$$

Manuscript received May 24, 1995, and revision received Jan. 2, 1996.